FQPSK-B [1] Baseband Filter Alternatives

Robert Jefferis
TYBRIN Corporation

ABSTRACT

Designers of small airborne FQPSK-B (-*B*) transmitters face at least two significant challenges. First, many U.S. Department of Defense (DOD) test applications require that transmitters accommodate a continuum of data rates from 1, to at least 20 Mb/s in one design. Another challenge stems from the need to package a high-speed digital baseband signal generator in very close proximity to radio frequency (RF) circuitry required for 1.4 to 2.4 GHz operation. The -*B* baseband filter options prescribed by Digcom/Feher [2] are a major contributor to variable data rate design challenges. This paper summarizes a study of -*B* filter alternatives and introduces FQPSK-JR (JR), an alternative to -*B* that can simplify digital baseband transmitter designs. Very short impulse response digital filters are used to produce essentially the same spectral efficiency and nonlinear amplifier (NLA) compatibility as -*B* while preserving or improving detection efficiency (DE). In addition, a strategy for eliminating baseband shaping filters is briefly discussed. New signaling wavelets and, modified wavelet versus symbol sequence mapping rules associated with them, can be captured from a wide range of alternative filter designs.

KEY WORDS

FQPSK-B, FQPSK-JR, baseband signal generator, FIR filter

INTRODUCTION

In 2000 the DOD adopted -*B* modulation in its Telemetry Standard IRIG-106 (*106*) for aeronautical telemetry [3]. One example of a digital quadriphase -*B* baseband signal generator compatible with variable data rate operation is shown in figure 1. FQPSK-B is created by application of the"-*B"* filters to FQPSK-KF (KF) waveforms produced by the wavelet selector. In this configuration, KF and "enhanced" FQPSK (EF) rely solely on wavelet characteristics and the anti-alias filters for baseband spectrum containment, i.e., the intervening low pass filter (LPF) is not used. [2] Figure 2 is an example of measured KF, EF, and -*B* NLA power spectra with a normalized sample rate ρ of 8 samples per symbol and no post digital to analog converter (DAC) image filter. The *106* -*B* power spectral density (PSD) mask is also shown. The curves match at frequency offsets up to about 0.55 times the bit rate r_b. Then they diverge and it is clear how -*B* attenuates out of band power. EF

[1] FQPSK-B refers to "Feher's patented Quadrature Phase Shift Keying" [1].
[2] A thorough description of KF waveforms, the cross-correlation function, and EF is given in Simon and Yan [4].

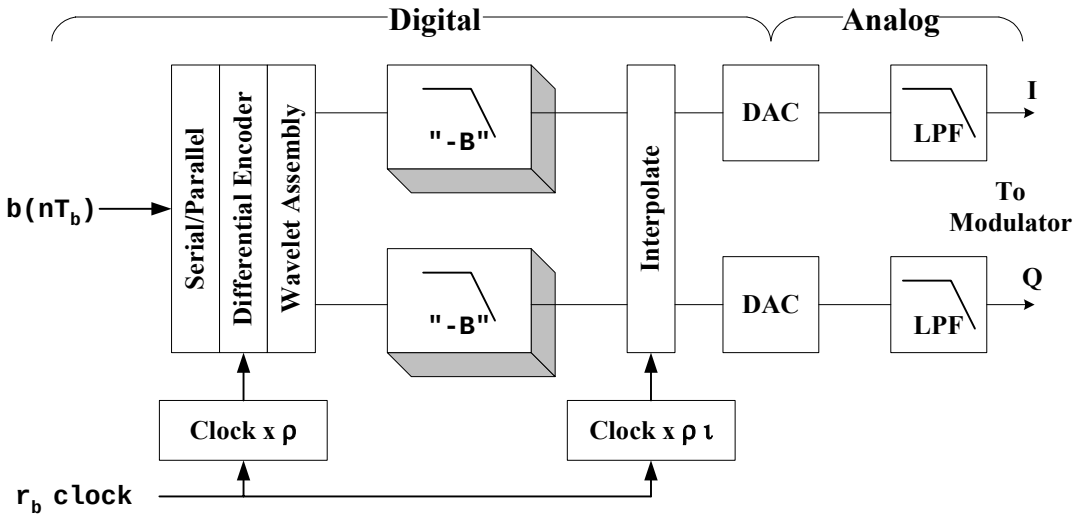

Figure 1: Baseband signal generator example.

spectra roll off faster than KF spectra above r_b but the EF bulge that appears at $0.6r_b$ has a significant impact on adjacent channel interference (ACI) performance. Some applications, like earth satellite links, can tolerate the adjacent channel power present in KF or EF spectra. Dense signal spacing in DOD test range applications cannot.

The structure of figure 1 is attractive because digital filter frequency response scales linearly and automatically with data rate. In addition, thoughtful manipulation of interpolation ratio ι can reduce

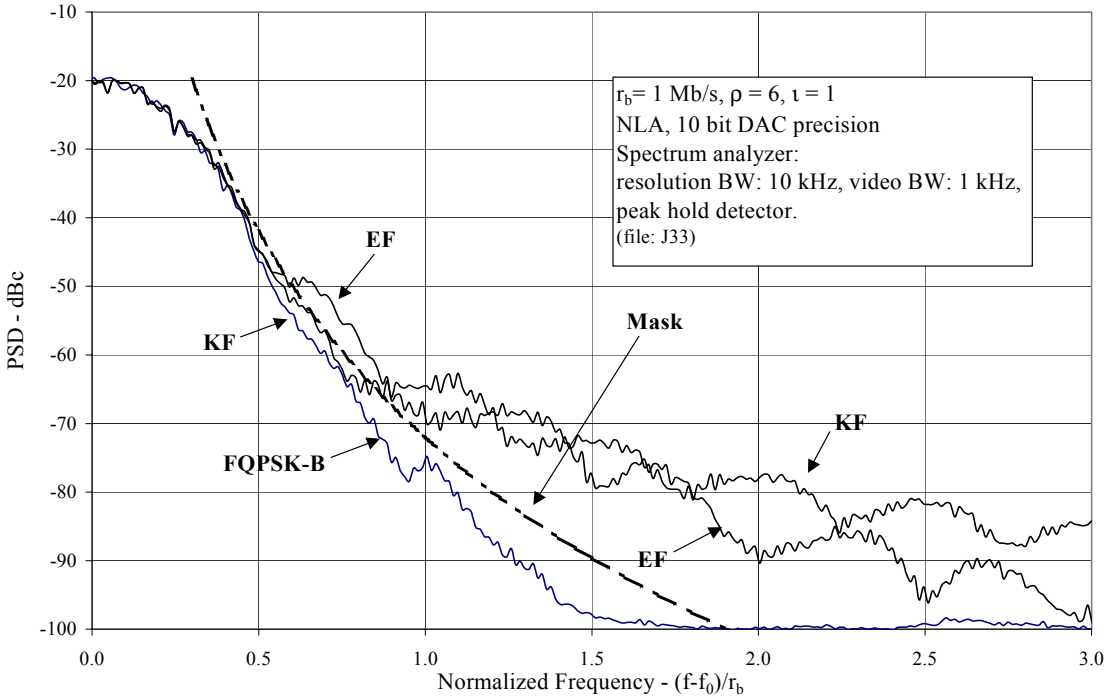

Figure 2: Baseline RF power spectra with NLA.

the DAC image filter to one fixed response requirement. Details of -*B* filters are proprietary. However, the obvious can be stated. In this configuration they are baseband LPFs selected to provide as much out of band attenuation as possible while minimizing main lobe distortion and retaining NLA compatibility. An inevitable side effect of such filtering is a small but tolerable amount of inter symbol interference (ISI). The -*B* filter prescription is quite effective, and is easy to implement in fixed rate analog designs. However, it becomes problematic in digital designs that must span over more than four octaves of bit rate variation in small physical packages. For example, the -*B* filter used for figure 2 requires 17 multiplies and 33 sums per sample. Clever design can simplify the filters somewhat, but in general, good -*B* filters are not trivial in terms of multiplier, gate count, and speed burdens. In the following sections alternative filter qualification criteria are discussed and the recommended result, referred to as FQPSK-JR, is presented in detail.

DEMONSTRATION SYSTEM

All data were acquired with the equipment shown in figure 3. The Rohde & Schwarz "AMIQ" I/Q Modulation Signal Generator and Agilent Technologies signal generator combine to make a powerful transmitter emulator. Cyclostationary sequences of desired I and Q channel waveforms are downloaded to the AMIQ from a custom MatLab™ program. In addition to providing a baseline for very high transmitter quality, the signal generator allows intentional degradation of phase noise and common quadrature modulator balance parameters. The signal generator drives a custom broadband class C NLA at 1.45 GHz. The signal is then translated to 70 MHz for additive white Gaussian noise (AWGN) injection. The intermediate frequency signal is demodulated and detected with commercial hard decision -*B* demodulators.

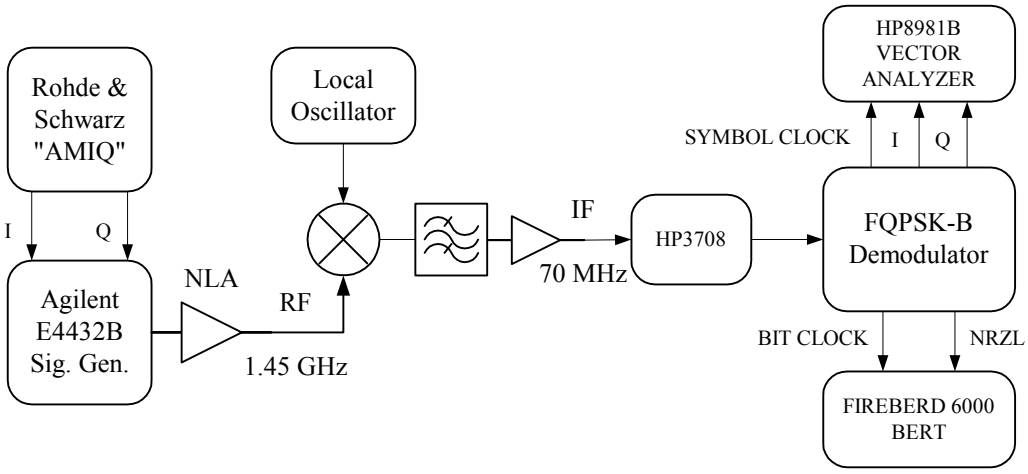

Figure 3: Test equipment.

ALTERNATIVE FILTER CRITERIA

The alternative filter study started with four assumptions: (1) the architecture of figure 1, (2) KF wavelets, (3) KF cross-correlation coefficient of 0.7071, and (4) cooperative, benign interpolation. In addition, three performance goals were adopted: (1) -*B* power spectra; (2) state-of-the-art hard decision -*B* AWGN DE benchmarks; and (3) baseband spurious emissions consistent with *106*, chapter 2. Preliminary experiments with -*B* showed that $\rho = 6$ should be the preferred sample rate when bit rate agility is desired. Results presented below confirm its adequacy. Lower rates degrade DE with the commercial benchmark demodulators and, required anti-alias filter specifications begin to approach "brick-wall" quality when $\iota = 1$.

The main lobe of -*B* is essentially that of a linearly amplified offset QPSK signal. With respect to non-Nyquist spectrum shaping filters and their impact on DE, experiments have shown that the frequency range over which waveform damage control must be enforced extends from zero to at least the 20 dB rolloff point of the modulated power spectrum or $f \cong 0.4r_b$. From this the critical *passband* range was conservatively set at $0 \le f \le 0.5r_b$ and a limit for combined shaping filter and interpolator attenuation was set at 3 dB, $f = 0.5r_b$. A "benign" interpolator was assumed to exhibit monotonic $\sin(af)/\sin(bf)$ passband response typical of common multiplierless interpolation schemes. A good example is the ubiquitous cascaded integrator-comb (CIC) interpolator [5]. A four-stage CIC interpolator was assumed with delay factor of unity and interpolation ratios in the range $1 \le \iota \le 32$. At $\rho = 6$, the worst CIC passband droop is 1.6 dB, $\iota = 32$. Thus, no more than about 1.4 dB of additional attenuation was allowed in alternate shaping filter designs at $f = 0.5r_b$.

Unfortunately, NLA and finite DAC precision effects prevent reliable prediction of spectral regrowth behavior at PSD levels of - 60 dBc and lower. Relations between filter transition band shape, stop band attenuation, and PSD response is highly nonlinear. For example, the difference between KF and -*B* power at $f = 1.5r_b$ in figure 2 is approximately 20 dB, but the -*B* filter provides more than 50 dB of attenuation at that point. The most efficient design approach is iterative evaluation of candidate filters with an emulator.

FQPSK-JR

Before describing the JR filter, a brief discussion of failures is in order. Approximately 40 variations of 12 alternative filters were tested. It is well known that recursive digital filters can provide good low pass frequency response characteristics with small numbers of filter weights. For the sake of completeness if nothing else, several recursive designs were tried. It was not surprising to find that attendant phase distortion produced unacceptable spectrum restoration. Phase compensation usually contained the regrowth but led to unattractive filter complexity. Finite impulse response (FIR) filters constrained to linear phase response were deemed the best prospects. At $\rho = 4$, 6,8, and $\iota = 1$, multiplierless comb and half-band filters introduce excessive passband droop with attendant DE loss. The most promising results were obtained by placing a transmission zero in the filter transfer function in the range $0.6r_b \le f \le r_b$ to create a somewhat sharp transition band. Passband response was then adjusted by cascading a simple droop compensation filter. Stopband performance was

evaluated in terms of PSD response with the emulator. Surviving candidates were then evaluated for integer arithmetic simplicity.

Any FIR filter can be described in terms of its impulse response sequence $h(n)$ with the z transform [6]:

$$\boldsymbol{H}(z) = \sum_{n=0}^{N-1} \boldsymbol{h}(\boldsymbol{n}) z^{-n} \qquad (1)$$

The equivalent composite impulse response of the preferred result, referred to as the JR filter, is shown in column 2 of table 1.

Table 1: JR Filter Impulse Response

filter weight	JR_{equiv}	JR_a	JR_b
h(0)	-0.046875	2^{-2}	$-(2^{-3} + 2^{-4})$
h(1)	0.109375	h(0)	$(2^{-1} + 2^{-3})$
h(2)	0.265625	h(0)	h(1)
h(3)	h(2)	-	h(0)
h(4)	h(1)	-	-
h(5)	h(0)	-	-

Its group delay is constant (3.5 samples) and it decomposes into the cascaded pair of trivial filters defined in columns 2 and 3. Designers of fixed-point integer arithmetic processors will note that each of the constituent filters can be implemented without dedicated hardware multiplication structures. Typically, one overall scaling operation is needed to adjust joint filter and interpolation gain with respect to peak wavelet scaling. JR attenuation, after scaling to unity gain at $f = 0$, is plotted in figure 4. Combined JR/CIC response at $\iota = 2$ and 32 is also shown. Additional passband droop introduced by the anti-alias filter should be limited to about 0.5 dB to avoid measurable degradation of DE.

The JR configuration involves one more factor. Mathematically, KF only produces constant envelope operation at mid symbol sampling instants when the cross-correlation coefficient A is [1, 2]:

$$\boldsymbol{A} = 1/\sqrt{2} \qquad (2)$$

During this study it was found that NLA PSD is not materially effected by varying A in the approximate range $0.69 \le A \le 0.75$. Theoretically, increasing A has the beneficial effect of improving DE. However, it was found that modest increases also improve out of band attenuation in the range $1.0 < \Delta f < 1.5$. The JR data presented below utilized **$\boldsymbol{A = 0.73}$** which is regarded as the best overall compromise of PSD rolloff, ACI sensitivity, and DE performance options.

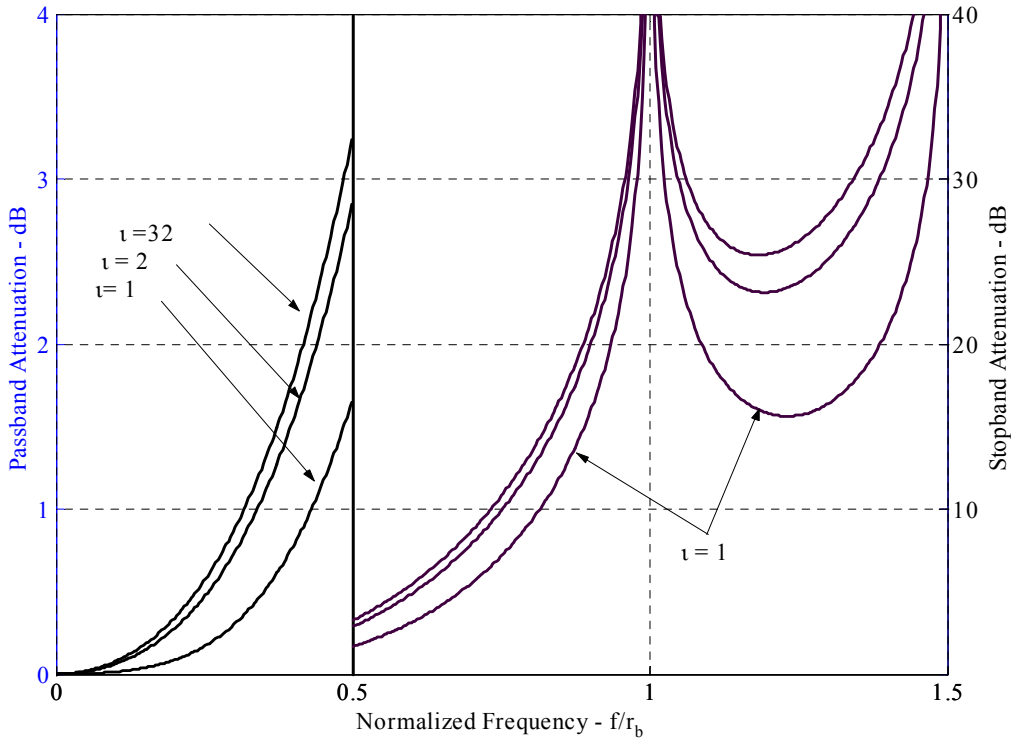

Figure 4: Solid lines are the JF frequency response. Broken lines are combined response of JF filter and 4-stage CIC filter at interpolation ratios of 2 and 32.

Figures 5 and 6 are JR power spectra. Notable deviations from -*B* only occur in the range $1.3 \le \Delta f \le 1.7$, $\iota = 1$. This degradation is not likely to be significant in practical situations because the image filter should provide significant additional attenuation in this range.

With respect to *106* recommendations, PSD plots are only indicative of general signal quality and spurious emission potential close to the carrier. The important measure of spectrum containment is ACI sensitivity. Figure 7 contrasts -*B* and JR in terms of a proposed *106* ACI criterion which states that the value of E_b/N_0 required for a bit error probability (BEP) of 1×10^{-5} shall not increase by more than 1 dB with respect to the AWGN DE value of E_b/N_0 for the same BEP, when an interfering -*B* signal of like bit rate, 20 dB stronger than the victim, is placed at $\Delta f = r_b$ Hz above or below the victim. The results show that JR matches -*B* at the specification point and is only 0.2 dB worse at $\Delta f = 0.95 r_b$.

Figure 8 shows that JR filters provide adequate headroom for practical modulator defects. The magnitude of impairments used for this example are each near the limits of good QPSK design practice.

Figure 9 is a plot of AWGN DE with benchmark demodulators (no anti-alias filter). Both demodulators use sharp front end filtering and narrow detection filters to remove the DAC images. Aside from the obvious absolute difference between demodulator designs, we see that JF is certainly equivalent to –*B*.

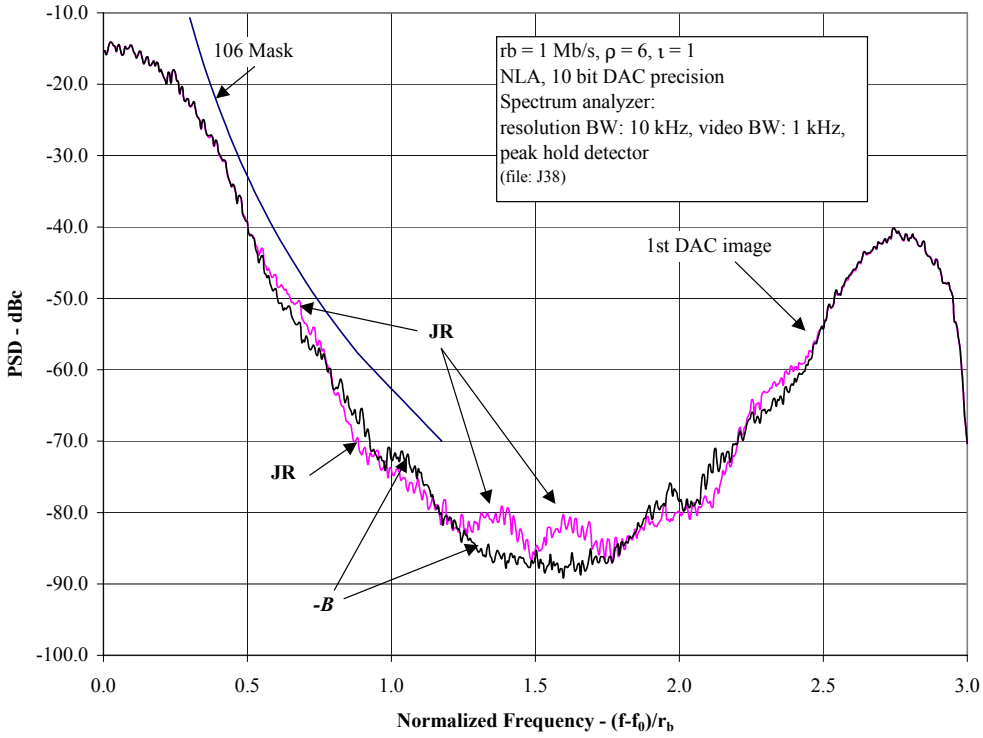

Figure 5: JR versus *–B* baseline PSD, no interpolation, no image filter.

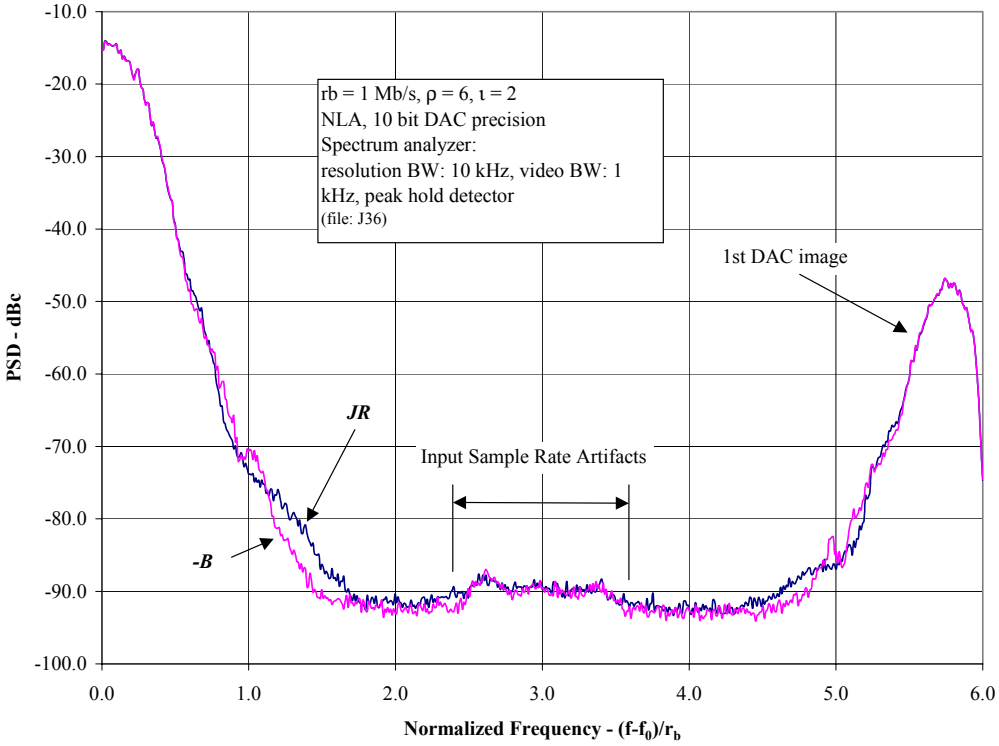

Figure 6: JR versus *–B* baseline PSD, with interpolation, no image filter.

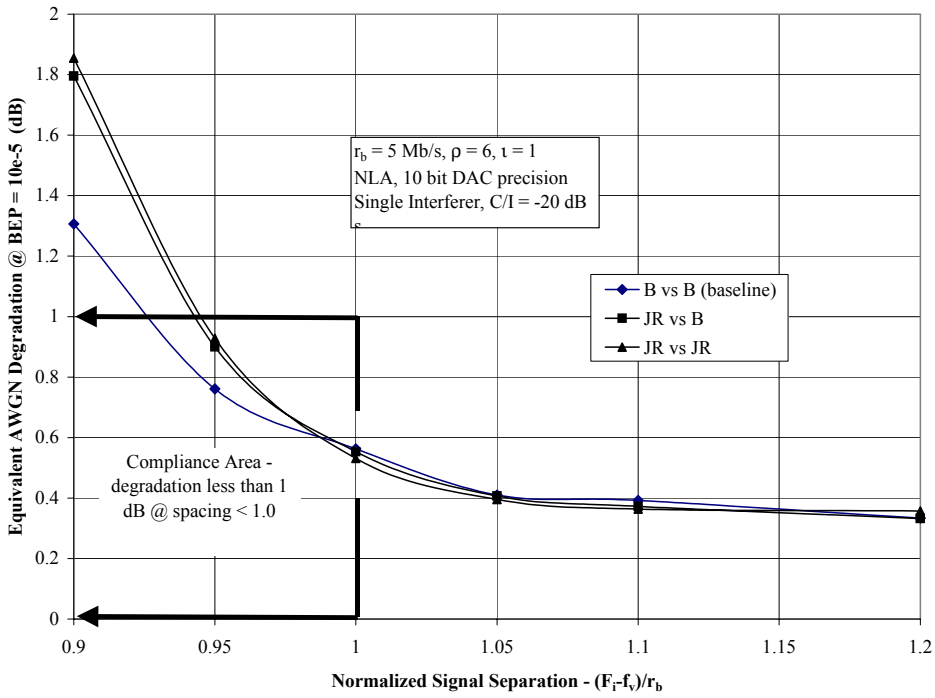

Figure 7: JR ACI performance with benchmark demodulator.

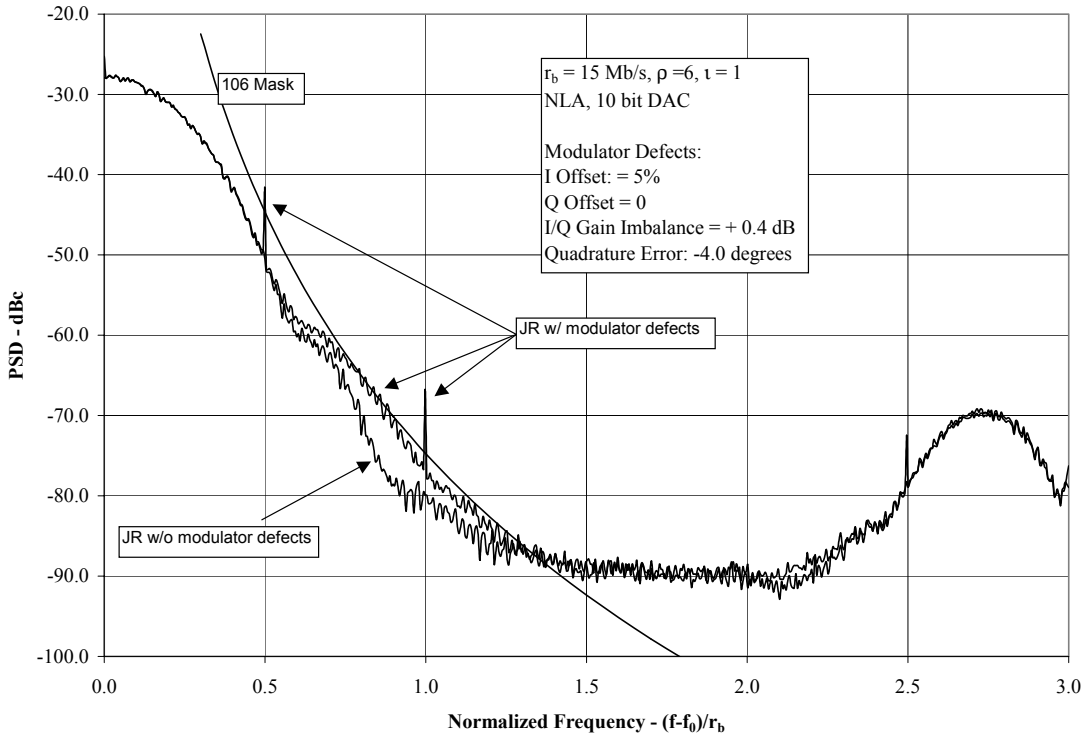

Figure 8: Example of I/Q modulator defect impact.

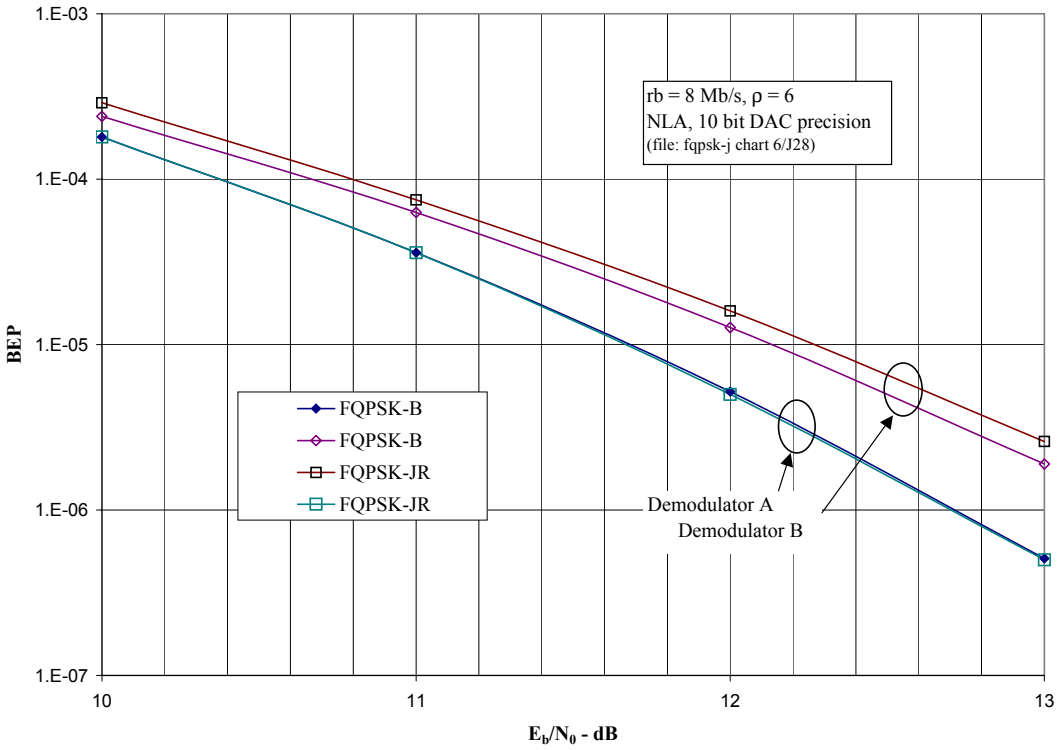

Figure 9: AWGN detection performance, hard decision detectors, differential encoding.

For completeness, comparative spectra produced by a complete processor example are shown in figure 10. A Krohn-Hite model 3955, 4-pole, dual channel filter was used as an image filter. Its -3 dB cutoff frequency was set at $1.13r_b$. Note that spectral growth becomes slightly asymmetric below -70 dBc. Such behavior has been found typical of interaction between NLAs, filtered FQPSK waveforms and image filters that are not phase compensated. Nonetheless, we see that a simple image filter can be effective as the final spectrum containment element if one is not seeking the ultimate in terms of out of band attenuation near the carrier.

SHAPING FILTER REMOVAL

Figure 11 is an ideal transmitter eye diagram of JR produced by the AMIQ load program. Aside from the larger opening (A= 0.73 vice 0.71), experienced FQPSK observers will find it indistinguishable from $-B$ without resorting to sophisticated test equipment. The only notable difference is lower level ISI and jitter due to very small JR filter group delay. Moreover, this means fewer vital waveform states, and it has been found practical to identify and capture all state variations. KF wavelet samples that would typically be stored in read only memory lookup tables within the "wavelet assembly" block of figure 1 can be replaced with samples of new wavelets associated with a different symbol sequence map. All pre-DAC filtering can thus be eliminated at the expense of larger lookup tables. An exhaustive state variation and corresponding input symbol sequence search program was developed that automatically produces the new wavelet sets (when a

unique set exists) and required bit rate symbol sequence mapping. Available space precludes presentation of number intensive

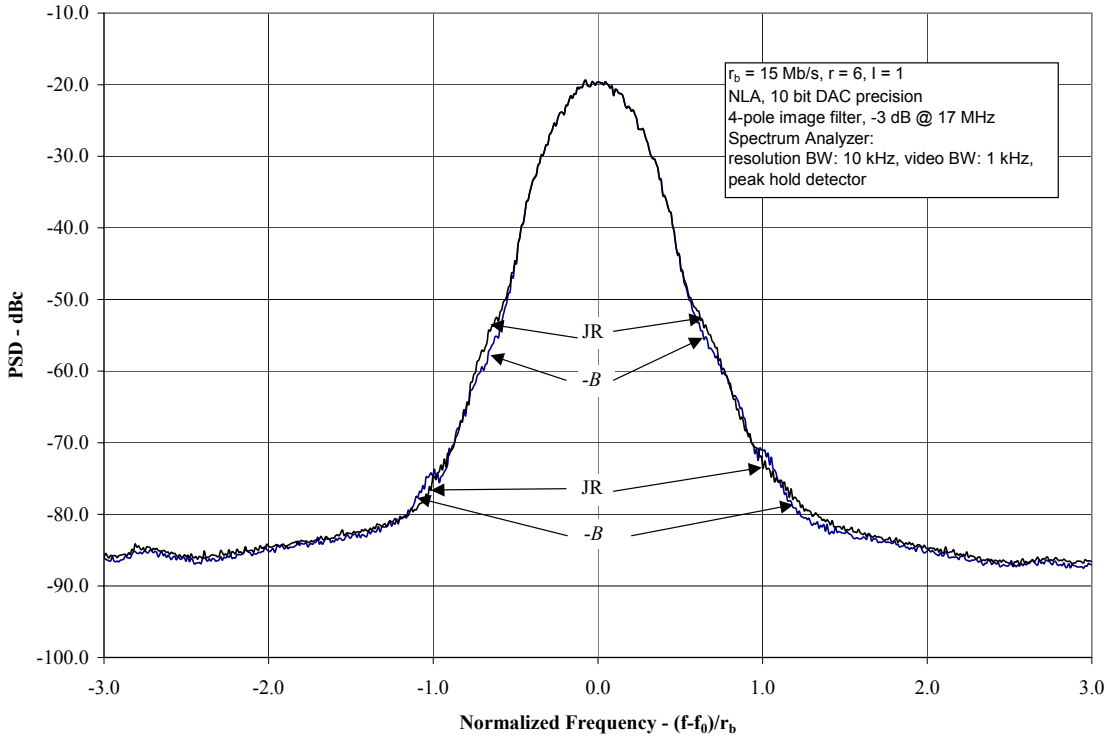

Figure 10: Example of complete JR and –*B* RF spectra with image filter and NLA.

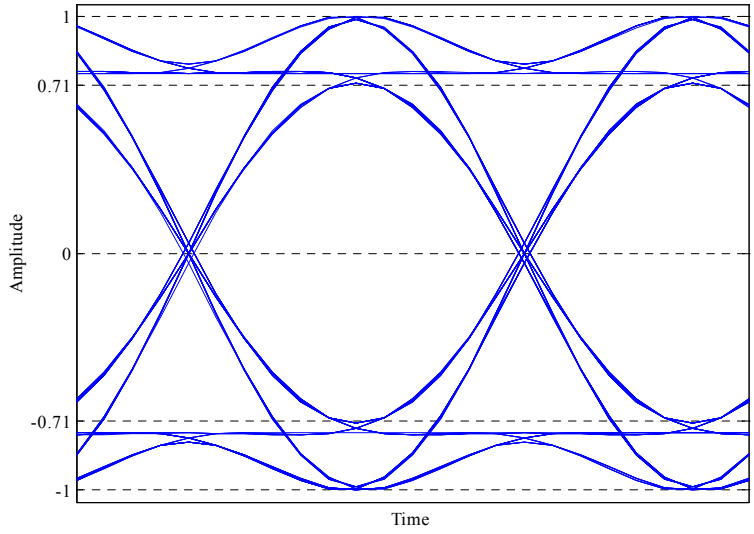

Figure 11: FQPSK-JR baseband generator eye diagram, I or Q channel, ι = 2, *A* = 0.73.

tables, however, numerous filterless examples have been created and executed in the emulator. In each case, at least to the extent detectable with measurement uncertainties, all performance characteristics of the filterless, table based implementation match those of the underlying run-time

filter version. Simplified, sub-optimum wavelet sets can readily be created as well, and trades of table size and mapping complexity versus system performance compromise are easily evaluated.

CONCLUSION AND ACKNOWLEDGEMENTS

The JR filter is an almost transparent substitute for -*B* filters. A member of the FQPSK family of cross-correlated OQPSK waveforms, JR retains the pseudo constant envelope characteristics of -*B* and consequent NLA compatibility while preserving DE and ACI performance. Its main benefit is significant simplification of baseband filter complexity in digital baseband signal generators. Use of its *specific* definition in transmitter specifications can result in uniform expectations for signal characteristics. A complete JR prototype modulator having all *digital* functions contained within one moderate complexity field programmable gate array is under construction.

This work was sponsored by the DOD tri-service Advanced Range Telemetry project, Edwards Air Force Base, California. Thanks are offered to Mr. "Rich" Formeister (RF Networks Inc., Phoenix, Arizona) for his assistance and insight and, to Mr. Eugene Law (U.S. Navy, NAVAIR, Weapons Division, Pt. Mugu, California) for the ACI data. The "JR" suffix was suggested by Mr. Feher and is consistent with his theme of labeling certain specific FQPSK variants with initials of people responsible for the development, which in this case are, Robert Jefferis and Richard Formeister.

REFERENCES

[1] Feher, K. et al., U.S. patents: 4,567,602; 4,339,724; 4,664,565; 5,784,402; 5,491,457. Canadian patents: 1,211,517; 1,130,871; 1,265,851.
[2] Feher, K., "FQPSK-B Revision A1 – Issue 2," Digcom-Feher Patented Technology Transfer Document, revised 15 June 2000, Digcom Inc, El Macero, California.
[3] "IRIG STANDARD 106-01," *TELEMETRY STANDARDS*, Vol. 1, Secretariat, Range Commanders Council, White Sands Missile Range, New Mexico, January 2000.
[4] Simon, M. and Yan, T-Y, "Unfiltered FQPSK: Another Interpretation and Further Enhancements", Applied Microwave & Wireless, parts 1 and 2, February and March 2000.
[5] Hogenauer, E., "An Economical Class of Digital Filters for Decimation and Interpolation," IEEE Transactions on Acoustics, Speech, and Signal Processing, Vol. ASSP-29, No. 2, April 1981.
[6] Rabiner, L. and Gold, B., *Theory and Application of Digital Signal Processing*, Prentice-Hall, New Jersey, 1975.

NOMENCLATURE

E_b/N_0	bit energy density to noise density ratio
f_0	carrier frequency
f_i	carrier frequency on interfering signal, ACI test
f_v	carrier frequency on victim signal, ACI test
ι	ratio of output sample rate to input rate
ρ	normalized sample rate, samples per symbol
r_b	bit rate